crystals

MDPI

Article

Effect of B_2O_3 on the Radiation Shielding Performance of Telluride Lead Glass System

Shiyu Yin [1,*], Hao Wang [1], Shifeng Wang [2,*], Jing Zhang [3] and Yuanzhi Zhu [1]

[1] School of Mechanical and Materials Engineering, North China University of Technology, Beijing 100144, China; xizaidaoren@163.com (H.W.); psbydyx@163.com (Y.Z.)
[2] Key Laboratory of Cosmic Rays, Ministry of Education, Tibet University, Lhasa 850000, China
[3] School of Information, North China University of Technology, Beijing 100144, China; whxsyh@163.com
* Correspondence: yinsy@ncut.edu.cn (S.Y.); wangsfac@163.com (S.W.)

Abstract: This paper studies the role of B_2O_3 in the radiation shielding properties of (100-x)(60TeO_2-40PbO)-xB_2O_3 glass systems where x = 0, 1, 2, 3, 4 and 5 mol%. Through the scanning electron microscope (SEM) and X-ray diffraction (XRD) tests of the glass, the structure of the glass was studied. Physical radiation sources (^{57}Co, ^{60}Co, ^{137}Cs, ^{133}Ba, and ^{241}Am) and WinXCOM software were used to experimentally and theoretically calculate the radiation properties of the glass, respectively. The gamma shielding ability of the glass was evaluated using its mass decay coefficient (μ_m), half-value layer (HVL), mean free path (MFP) and effective atomic number (Z_{eff}). The neutron shielding ability of the glass was evaluated by calculating the fast neutron removal cross-section (RCS) value. The glass's gamma and neutron shielding properties were compared to various ordinary concrete and other tellurite glasses. The measured mass decay coefficients agree well with the theoretical values obtained using WinXCOM software. Low HVL, MFP, and high μ_m, Z_{eff}, and RCS values indicate that this series of glass materials have good shielding properties. According to the obtained results, among the glass samples doped with B_2O_3, the TPB-1 glass sample showed the best radiation shielding performance.

Keywords: radiation-shielding; telluride glass; high-energy rays

Citation: Yin, S.; Wang, H.; Wang, S.; Zhang, J.; Zhu, Y. Effect of B_2O_3 on the Radiation Shielding Performance of Telluride Lead Glass System. *Crystals* **2022**, *12*, 178. https://doi.org/10.3390/cryst12020178

Academic Editor: Alessandro Chiasera

Received: 4 January 2022
Accepted: 21 January 2022
Published: 26 January 2022

1. Introduction

Human application of radiation involves all aspects of production and life, such as radiographic research, radiotherapy, academia, the food industry, and gas detectors and safety devices. However, in addition to the benefits of nuclear energy, the harm caused by radiation to the human body and the environment cannot be ignored [1–3].

Radiation has a strong ability to penetrate the human body, which can directly cause damage to the human body or indirectly cause damage to future generations through deformation and inheritance. Therefore, people have made extensive efforts to reduce the harm of ionizing radiation. One of them is to explore shielding materials, which attracts researchers to manufacture new shielding materials [4–6].

At present, the most commonly used radiation shielding materials are lead and concrete, but these materials have their disadvantages. For example, pure lead bricks are opaque and toxic, and concrete density will decrease over time [7,8]. Therefore, researchers will pay attention to tellurite glasses and study some tellurite glasses containing different heavy metal oxides, such as PbO, MgO, Ag_2O, Nb_2O_5, ZnO and BaO [9–11] Tellurite glass has excellent properties such as transparency in a wide wavelength range, good thermal stability, non-hygroscopicity, low melting temperature, chemical durability, and high refractive index. Among the studied tellurite glasses, the PbO-doped glasses show the lowest MFP values (best shielding properties) [12]. However, the structural stability of pure TeO_2-PbO glass is poor, which is not conducive to further processing. Therefore, adding a strong glass former B_2O_3 to the glass composition has become an excellent choice

to optimize the glass structure. However, at the same time, a large amount of B_2O_3 cannot be doped to the glass. Otherwise, the glass's density and radiation shielding ability will be significantly reduced [13–15].

This work studied the influence of B_2O_3 content on the structure and radiation shielding performance of (100-x)(60TeO_2-40PbO)-xB_2O_3 (where x = 0, 1, 2, 3, 4 and 5 mol%) glass systems. Through scanning electron microscopy (SEM) and X-ray diffraction (XRD) studied the structure of the glass. Using ^{57}Co (0.122 MeV), ^{60}Co (1.173 and 1.332 MeV), ^{137}Cs (0.662 MeV), ^{133}Ba (0.081 and 0.356 MeV), and ^{241}Am (0.059 MeV) as radioactive sources to evaluate the linear attenuation coefficient (μ) of these glasses, and using WinXCOM software to verify the accuracy of the test results, the μ_m value, the half-value layer (HVL) and mean free path (MFP) are evaluated. The electronic radiation shielding characteristics are tested by measuring the effective atomic number (Z_{eff}) of the glass involved. The neutron radiation shielding properties are discussed by theoretical calculation of the studied glass's fast neutron removal cross-section (RCS).

2. Materials and Methods

2.1. Sample Preparation

The (100-x)(60TeO_2-40PbO)-xB_2O_3 (where x = 0, 1, 2, 3, 4 and 5 mol%) glass were synthesized by conventional melt quenching technology and named TPB-0, -1, -2, -3, -4, and -5 using TeO_2, PbO, and H_3BO_3 (99.99%). We mix them evenly after weighing. The raw materials of each glass were placed in a pure alumina ceramic crucible, melted at 850 °C and reacted for 2 h, and then the molten glass was cast on a plate-shaped brass mold preheated to 250 °C. The obtained solid glass was slowly cooled from 250 °C to room temperature at a cooling rate of 1 °C/min. Finally, the cooled glass is cut into glass blocks with a thickness of about 1.5 mm, and the cross-sectional size of each glass is about 20 × 10 mm. The two large glass surfaces are optically polished, and the thickness is measured.

2.2. Structure Stability Experiment

The structure of TPB series glass was characterized as follows: in the vacuum mode, the sample with gold spray treatment on the surface was tested with a high-resolution environmental scanning electron microscope (FEI Quanta 650, EI Company, Hillsboro, OR, USA) at an acceleration of 500 kV. With 2θ = 10°–80° diffraction angle and 0.02°/min rate, at room temperature, testing the X-ray diffraction (Ultima IV, Rigaku, Chiba, Japan) pattern of the sample. The density was measured with pure water (ρ = 0.99980 g/cm^3, 16 °C) as the regular temperature immersion liquid.

2.3. Radiation Shielding Experiment

The radiation shielding measurement device is shown in Figure 1. The radiation source is placed 300 mm away from the sample. We placed a collimator with an aperture of 5 mm between the radiation source and the sample. We surrounded the detector with a 20 mm thick lead brick to resist the radiation scattered by the radiation source and reduce the pollution of the surrounding environment.

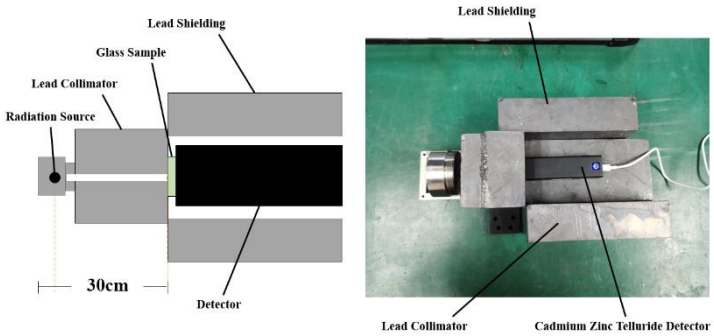

Figure 1. Structure diagram and physical diagram of the radiation shielding measurement device.

In this study, five radiation sources, ^{57}Co (0.122 MeV), ^{60}Co (1.173 and 1.332 MeV), ^{137}Cs (0.662 MeV), ^{133}Ba (0.081 and 0.356 MeV) and, ^{241}Am (0.059 MeV), were used to obtain collimated narrow gamma ray bundles with seven energies.

To reduce background radiation's influence on the experimental results, we let the detector work for 30 min without a radiation source to obtain the background radiation I_{bg} in the environment. For reducing the influence of random errors on the experimental results, each piece of glass was tested ten times under each radiation source. The counting time of each test is 5 min Finally, the counting rates I_0 with no glass placed and the count rate I after placing the glass obtained.

3. Calculation

The count rate obtained by detection before and after the glass is placed obeys the Lambert-Beer law [16]:

$$\mu = 1/t \times \ln\left[(I_0 - I_{bg})/(I - I_{bg})\right] \quad (1)$$

where t is the thickness of the glass sample tested.

The mass attenuation coefficient μ_m of the glass can be obtained by the following Formula (2):

$$\mu_m = \mu/\rho \quad (2)$$

where ρ is the density of the material.

The thickness of the shielding material that can reduce the beam intensity to 1/2 of the initial state is called the half-value layer HVL. It is a key shielding parameter related to material thickness and can be calculated by the following Formula (3) [17]:

$$HVL = \ln(2)/\mu \quad (3)$$

The mean free path MFP is an important parameter, which is a parameter for calculating the average distance between two subsequent collisions. MFP can be calculated with the following Formula (4) [18]:

$$MFP = 1/\mu \quad (4)$$

The effective atomic number Z_{eff} value of the material can be determined by direct calculation method [19]. We use the data of the famous XCOM database to theoretically calculate the Z_{eff} value. We have selected 26 photon energies commonly used in radiation shielding studies in the energy range of 0.01–15 MeV, and calculated the corresponding Z_{eff} value.

$$Z_{eff} = \left(\sum_i f_i A_i \mu_{mi}\right)/\left(\sum_i f_i A_i \mu_{mi}/Z_i\right) \quad (5)$$

where f_i is the molar fraction, A_i is the atomic weight, and the Z_i is the atomic number.

To evaluate the neutron radiation shielding ability of TPB series glass, we calculated the RCS value of the fast neutron removal cross section of each component glass and compared it with the commonly used neutron shielding materials. The RCS value reflects the material's ability to block neutron beams. The higher the RCS value, the better the ability of the material to prevent neutron radiation. The formula for calculating the RCS value is as follows [20,21]:

$$RCS = \sum_i \rho_i \left(\sum R/\rho\right)_i \quad (6)$$

where ρ_i is the partial density of the i constituent and the $\sum R/\rho$ the mass removal cross section.

4. Results and Discussion

4.1. Structural Properties

The XRD diffraction pattern of the TPB glass is shown in Figure 2. It can be seen from Figure 2 that when x = 1 and 5, the X-ray images of the glass frit are the same. They have broad diffraction peaks around $2\theta = 30^\circ$ and $2\theta = 50^\circ$ in the diffraction patterns, respectively, without very sharp diffraction peaks, which are very typical diffraction patterns of amorphous substances. This XRD pattern shows that when the molar percentage of

B_2O_3 is between 1% and 5%, the product obtained after melting the TPB glass system is an amorphous glass body. When x = 0, it can be seen from the XRD pattern that there are crystallization peaks in the glass sample, which is the precipitation of a small amount of TePb crystals. This phenomenon shows that the addition of B_2O_3 can effectively reduce the crystallization tendency of glass.

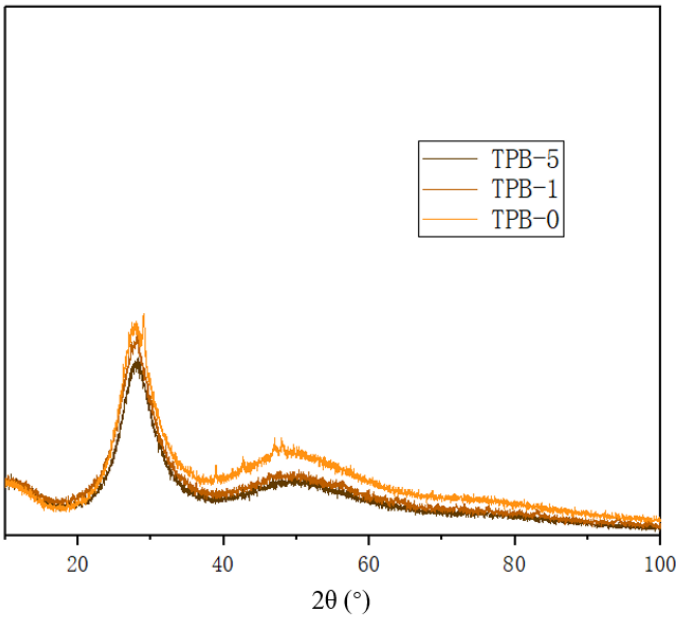

Figure 2. X-ray diffraction (XRD) pattern of TPB series glass.

For pure glass materials, the generation of crystal phase means that at the crystallization point, the structure and mechanical strength of the glass will change abruptly, making the glass easy to break at the crystallization point, which reduces the overall mechanical strength of the glass and increases the difficulty of processing, and not conducive to the preparation of glass products.

The unpolished samples of TPB-0, TPB-1 and TPB-5 after casting are shown in Figure 3. The TPB glass is a series of transparent, light yellow-green glass. The glass surfaces of TPB-1–TPB-5 are all light-transmitting and well-structured. The glass surface of TPB-0 is also light-transmitting, but there are apparent crystallization points as shown in Figure 3b. As can be seen from the figure, the TPB-0 sample was broken into more than a dozen small pieces, while the TPB-1 and TPB-5 samples were a complete large piece. This phenomenon is because TPB-1–TPB-5 are doped with B_2O_3. As a strong glass former, B_2O_3 helps to optimize the glass's mechanical properties and helps obtain a larger volume of glass for subsequent processing.

Figure 3. TPB-0 (**a**,**b**), TPB-1 (**c**), and TPB-5 (**d**) glass samples after casting.

The structure of the glass can also be discussed in terms of the thickness of the glass produced. The thickness of the polished glass is shown in Table 1. Grinding the glass to a thickness of about 1.5 mm is because the thickness of TPB-1–TPB-5 after pouring is between 1.6 mm and 1.8 mm, and the thickness of TPB-0 glass after casting is about 0.8 mm. As mentioned above, the glass in this study is prepared by conventional melt quenching technology. In this preparation method, the molten glass is poured on a brass mold, and the molten glass is waited for without artificial interference under the condition of air cooling, the flow spreads and solidifies into a block glass. Under the same total mass and cooling conditions, the higher the viscosity of the glass, the lower the rate of flow and extension of the glass liquid, and the greater the thickness of the final glass. Since TPB-0 is not doped with B_2O_3, a strong glass former, it has low viscosity and a large extension area during casting, so its thickness is much smaller than other B_2O_3-doped glasses.

Table 1. Compositions, density, and thickness of glass sample.

Sample Code	Mole Fraction/%			Density	Thickness	Wt. Fraction of Elements in Each Sample			
	TeO_2	PbO	B_2O_3	d/(g·cm^{-3})	t(mm)	B	O	Te	Pb
TPB-0	60.0	40.0	0.0	6.5917	0.756	0	0.138348	0.413748	0.447903
TPB-1	59.4	39.6	1.0	6.5498	1.506	0.001176	0.140435	0.412182	0.446207
TPB-2	58.8	39.2	2.0	6.4605	1.522	0.002366	0.142548	0.410596	0.444490
TPB-3	58.2	38.8	3.0	6.3277	1.510	0.003572	0.144688	0.408989	0.442751
TPB-4	57.6	38.4	4.0	6.2640	1.535	0.004793	0.146855	0.407362	0.440990
TPB-5	57.0	38.0	5.0	6.1984	1.516	0.006030	0.149050	0.405714	0.439206

4.2. Density

The composition, density and thickness of TPB series glass are shown in Table 1. From TPB-0 to TPB-5, the density of the glass gradually decreased from 6.5917 g/cm^3 to 6.1984 g/cm^3. This is because the addition of B_2O_3 can make the glass structure more compact. The molar mass of B_2O_3 (69.62 g/mol) is significantly lower than that of TeO_2 (159.6 g/mol) and PbO (223.2 g/mol). Therefore, the density of glass decreases with the increase of B_2O_3 content. For radiation shielding materials, density is an important parameter closely related to the values of μ_m, HVL and MFP. Generally speaking, the denser the glass, the stronger its radiation shielding properties, which means more atoms and electrons per unit volume of the material can interact with gamma rays. The higher the probability of interaction, the stronger the shielding ability of the material to gamma rays. The density of TPB series glass is above 6.1 g/cm^3, which is a typical high-density glass, so this series of glass is suitable for use as a gamma radiation shielding material.

4.3. Mass Attenuation Coefficient

To verify the accuracy of the μ_m value obtained from the test, we use WinXCOM software to simulate the μ_m value of TPB series glass within the range of 0.05–1.5 MeV photon energy and compare the experimental data $(\mu_m)_{Exp}$ compared with the data simulated by WinXCOM software $(\mu_m)_{XCOM}$. Calculate the relative difference (Dev) between the two methods according to the following formula:

$$\mathrm{Dev} = \left| [(\mu_m)_{Exp} - (\mu_m)_{XCOM}] / (\mu_m)_{XCOM} \right| \times 100\% \quad (7)$$

The values and errors of the two are shown in Table 2. From the data in the table, it can be known that the Dev values of the six glass types are all less than 5%, which verifies the accuracy of the experimental results.

Table 2. Compare the mass attenuation coefficient values μ_m (cm^2/g) obtained by the TPB series glass experiment and WinXCOM simulation.

Energy (MeV)		TPB-0	TPB-1	TPB-2	TPB-3	TPB-4	TPB-5
0.059	XCOM	5.4235	5.3583	5.2959	5.2330	5.1700	5.1080
	Exp	5.6363	5.4266	5.3587	5.3262	5.2015	5.1822
	Dev	3.78%	1.26%	1.17%	1.75%	0.61%	1.43%
0.081	XCOM	2.3770	2.3501	2.3236	2.2970	2.2700	2.2440
	Exp	2.4871	2.3890	2.3565	2.3075	2.2780	2.2832
	Dev	4.43%	1.63%	1.40%	0.45%	0.35%	1.72%
0.122	XCOM	1.9716	1.9525	1.9302	1.9080	1.8860	1.8650
	Exp	2.0041	1.9871	1.9394	1.9318	1.9029	1.8966
	Dev	1.62%	1.74%	0.47%	1.23%	0.89%	1.66%
0.356	XCOM	0.1975	0.1965	0.1953	0.1941	0.1929	0.1917
	Exp	0.2044	0.1991	0.1968	0.1979	0.1956	0.1939
	Dev	3.40%	1.32%	0.77%	1.94%	1.39%	1.13%
0.662	XCOM	0.0908	0.0907	0.0905	0.0903	0.0901	0.0899
	Exp	0.0947	0.0924	0.0915	0.0921	0.0912	0.0906
	Dev	4.16%	1.89%	1.07%	1.94%	1.19%	0.74%
1.173	XCOM	0.0571	0.0571	0.0571	0.0571	0.0571	0.0571
	Exp	0.0580	0.0581	0.0578	0.0581	0.0578	0.0578
	Dev	1.50%	1.76%	1.12%	1.65%	1.20%	1.24%
1.332	XCOM	0.0527	0.0527	0.0527	0.0527	0.0527	0.0526
	Exp	0.0538	0.0533	0.0529	0.0529	0.0537	0.0535
	Dev	2.17%	1.21%	0.52%	0.36%	1.79%	1.51%

The μ_m profile of the TPB is shown in Figure 4. It can be seen that the two quantities that determine the value of μ_m are the value of incident photon energy E_p and the content of B_2O_3 in the range of 0.059 MeV < E_p < 1.332 MeV.

In the whole range, the value of μ_m of TPB glass decreases with the increase of E_p, and the decreasing trend is an exponential decrease. When the B_2O_3 content increases, the μ_m value decreases. However, the B_2O_3 content has different effects on the μ_m value under different E_p conditions. The influence of B_2O_3 content on the μ_m value is more evident in the range of E_p < 0.662 MeV. For example, the μ_m value of TPB-1 is 5.3583 cm^2/g, and the μ_m value of TPB-5 is 5.1080 cm^2/g, at E_p = 0.059 MeV, which is quite different. The influence of B_2O_3 content on μ_m value is greatly reduced in the range of $E_p \geq 0.662$ MeV. For example, the μ_m value of TPB-1 is 0.0527 cm^2/g, and the μ_m value of TPB-5 is 0.0516 cm^2/g at E_p = 1.332 MeV, which is almost the same.

This phenomenon is because gamma photons interact with matter in different forms under different incident photon energies. When gamma rays pass through the material, the gamma photons will interact with the atoms in the material and lose most of their energy. Therefore, the difference in interaction will affect the radiation attenuation results. The interaction between gamma photons and matter mainly includes the photoelectric effect, Compton, and electron pair effect. For TPB series glass, the main interaction mode is the photoelectric effect when E_p is lower than 0.662 MeV, and the Compton effect dominates when E_p is higher than 0.662 MeV. Compared with the photoelectric effect, the Compton effect is less dependent on the material's atomic number. Therefore, the μ_m value will decrease with the increased B_2O_3 content in the area dominated by the photoelectric effect.

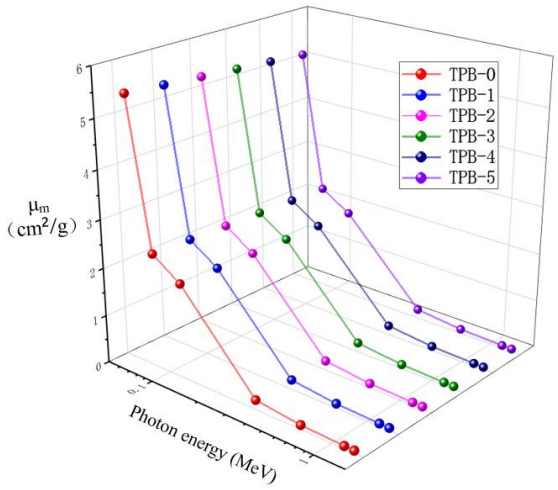

Figure 4. Mass attenuation coefficients (μ_m) of TPB glass system as a function of the photon energy and the chemical composition.

4.4. Half-Value Layer and Mean Free Path

In nuclear physics, HVL and MFP are essential variables used to describe the gamma shielding ability of material and the level of gamma radiation penetrating the environment. Materials withing lower HVL and MFP values can provide a better radiation shielding effect under the same thickness. Figure 5 shows the HVL value under different photon energy and chemical composition. TPB-5 with the highest B_2O_3 concentration has the highest HVL value compared with other samples. The HVL was enhanced with a photon energy between 0.059–1.332 MeV and attained their maximum values at about 1.332 MeV.

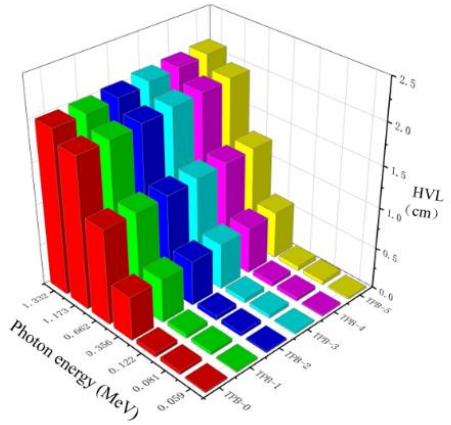

Figure 5. Half value layer (HVL) of TPB glass system under different photon energy and chemical composition.

In addition, we also investigated the mean free path MFP of the TPB series of glasses. The theoretically calculated MFP values of TPB-5 glass are compared with those of other radiation shielding glass materials, as shown in Figure 6. Similar to HVL, the smaller the MFP value, the better. As the value of MFP decreases, the distance between two successive interactions is smaller, which means that the attenuation ability of materials of equal thickness is more significant. Therefore, the MFP value can directly represent the performance of any gamma-ray shielding medium. It can be seen from Figure 6, the MFP value of TPB-5 with the largest MFP value in the TPB series is still lower than that of other tellurite glasses, which shows that TPB series glass has better radiation attenuation ability than other tellurite glasses for radiation shielding. It is more suitable to be used as a radiation shielding material.

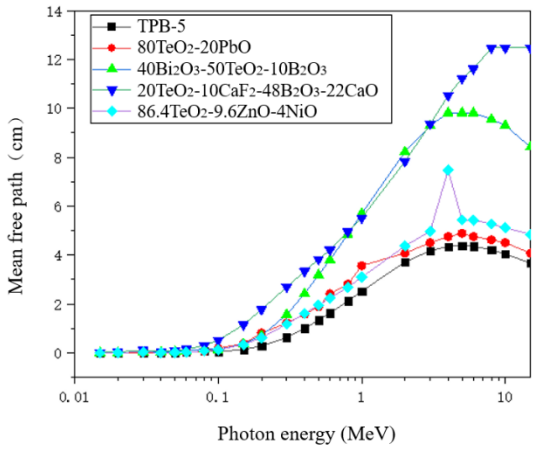

Figure 6. Comparison between the mean free path (MFP) for the TPB glasses with different radiation shielding glass.

4.5. Effective Atomic Number

The theoretically calculated effective atomic number Z_{eff} of the TPB glass is shown in Figure 7. The Z_{eff} value is an indispensable parameter in the study of gamma shielding, and it is another key factor in radiation physics. The magnitude of the Z_{eff} value reflects the gamma attenuation ability of the absorbent material. Objects with large Z_{eff} values are the preferred targets for more collisions of photons, so photons are highly attenuated in these materials. In actual shielding applications, anti-radiation glass with a high Z_{eff} value is more reliable for shielding gamma radiation.

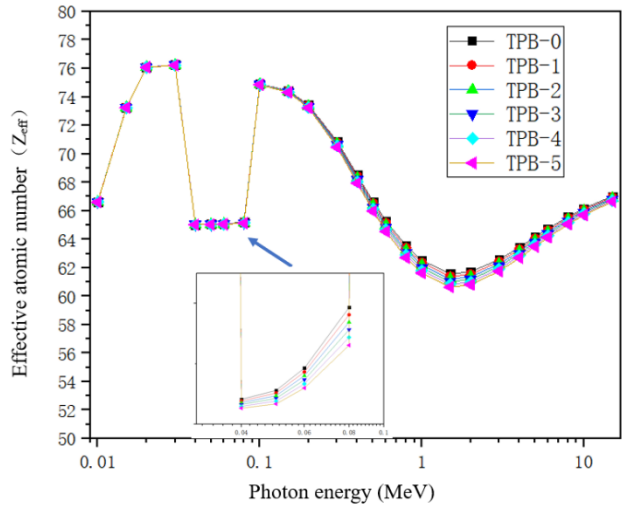

Figure 7. Effective atomic number (Z_{eff}) of TPB glass system for total electron interaction.

The Z_{eff} value of TPB glass increases with the increase of B_2O_3 content. In the TPB glasses, the highest Z_{eff} values occurred between 0.02 MeV and 0.03 MeV during the energy range of 0.01 MeV < E_p < 15 MeV. The reason is that the photoelectric equation governed the gamma interaction with Z^4 in its numerator. The high-Z elements (Te and Pb) have extremely high μ_m values at low E_p. Moreover, two abrupt changes in the Z_{eff} curve are derived from the photoelectric effect near the absorption K-edge of the Te element at 0.0318 MeV and that of the Pb element at 0.088 MeV. As E_p increases, the Z_{eff} of the glass gradually decreases because of the Compton scattering. Finally, the Z_{eff} value has a slight increase in the range of 3 MeV < E_p < 15 MeV because of the generation and annihilation process of the pair production.

It can also be observed that the glass Z_{eff} curves of the different glass compositions can be distinguished in the range of E_p > 0.1 MeV. However, the curves almost overlap

in the range of E_p < 0.1 MeV. This phenomenon is mainly affected by the change of μ_m value of each element. According to Formula (5), the Z_{eff} value depends on each element's atomic number and the product of the mass fraction and the μ_m value. As shown in Table 3, the values of $(\mu_m)_{Te}$ and $(\mu_m)_{Pb}$ are tens or even hundreds of times the value of $(\mu_m)_B$ in the range of E_p < 0.1 MeV. So, the increase of B_2O_3 has little effect on the Z_{eff} value in this range. Then with the increase of E_p, the ratio of the value of $(\mu_m)_{Te}$ and $(\mu_m)_{Pb}$ to the value of $(\mu_m)_B$ rapidly decreases to single digits, the decrease of Z_{eff} value by B_2O_3 content also becomes evident.

Table 3. Mass attenuation coefficient μ_m (cm^2/g) of B element, Ba element and Pb element.

E_p (MeV)	0.01	0.05	0.1	0.5	1	5	15
B	1.2550	0.1665	0.1391	0.0806	0.0589	0.0247	0.0149
Te	146.4	11.38	1.7920	0.0931	0.0566	0.0349	0.0429
Pb	130.6	8.041	5.5500	0.1613	0.0710	0.0427	0.0565

4.6. Removal Cross Section

The theoretically calculated RCS values of the TPB series glasses are shown in Figure 8. For comparison, the RCS values of graphite and ordinary concrete are also shown in Figure 8. Generally, the higher the RCS value, the better the neutron shielding performance of glass. The RCS values of TPB-0–TPB-5 are 0.10413, 0.10415, 0.10342, 0.10198, 0.10164 and 0.10126 cm^{-1}, respectively. With the increase of B_2O_3, the RCS value of glass decreases gradually. This phenomenon is because the lower atomic number B element in the glass component replaces the higher atomic number Te and Pb elements, which reduces the RCS value. The RCS value of TPB-5 is the smallest of TPB series glass. Still, it is generally higher than graphite and ordinary concrete, indicating that TPB series glass is more suitable as neutron radiation shielding material than graphite and ordinary concrete.

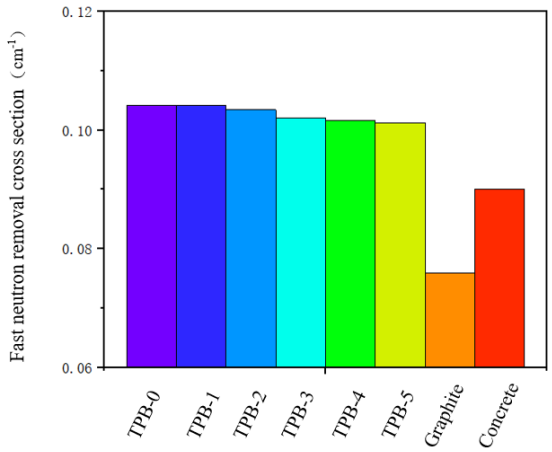

Figure 8. Removal cross section (RCS) of TPB series glass, graphite, and ordinary concrete.

5. Conclusions

This study tested the γ-ray and fast neutron radiation shielding ability of the (100-x)($60TeO_2$-40PbO)-xB_2O_3 glass system. The μ value is measured using a physical radiation source. Then, the μ_m, HVL, MFP, Z_{eff}, and RCS parameters of all selected glasses were calculated compared with ordinary commercial glass and concrete. With the increase of the proportion of B_2O_3 in the composition, the glass network structure is optimized, but its density and radiation shielding ability will also decrease. TPB-1 glass has the highest μ_m, Z_{eff} and RCS values, and the lowest HVL, MFP values. It has the best radiation shielding performance during TPB series glasses and is higher or equal to common radiation shielding materials. Therefore, it can be concluded that TPB series glass can be used as a new and high-quality radiation protection application shield.

Author Contributions: Conceptualization, S.Y. and S.W.; methodology, S.Y.; software, J.Z.; validation, H.W. and Y.Z.; formal analysis, H.W.; investigation, H.W.; resources, S.W.; data curation, H.W.; writing—original draft preparation, H.W.; writing—review and editing, H.W.; visualization, S.W.; supervision, S.Y.; project administration, S.Y.; funding acquisition, S.Y. All authors have read and agreed to the published version of the manuscript.

Funding: This research was funded by the Scientific Research Project of Beijing Educational Committee, grant number 110052971803/069; the National Natural Science Foundation of China, grant number 52062045 and 12047575; and the Central Government Funds for Local Scientific and Technological Development, grant number XZ202101YD0019C.

Conflicts of Interest: The authors declare that they have no conflict of interest.

References

1. Rammah, Y.; El-Agawany, F.; Abu El Soad, A.; Yousef, E.S.S.; El-Mesady, I. Ionizing Radiation Attenuation Competences of Gallium Germanate-Tellurite Glasses Utilizing MCNP5 Simulation Code and Phy-X/PSD Program. *Ceram. Int.* **2020**, *46*, 22766–22773. [CrossRef]
2. Hamad, R.; Mhareb, M.; Alajerami, Y.; Sayyed, M.; Saleh, G.; Hamad, M.K.; Ziq, K. A Comprehensive Ionizing Radiation Shielding Study of FexSe0.5Te0.5 Alloys with Various Iron Concentrations. *J. Alloy. Compd.* **2021**, *858*, 157636. [CrossRef]
3. Olarinoye, I.; Alomairy, S.; Sriwunkum, C.; Al-Buriahi, M.S. Effect of Ag_2O/V_2O_5 Substitution on the Radiation Shielding Ability of Tellurite Glass System via XCOM Approach and FLUKA Simulations. *Phys. Scr.* **2021**, *96*, 065308. [CrossRef]
4. Boonin, K.; Yasaka, P.; Limkitjaroenporn, P.; Rajaramakrishna, R.; Askin, A.; Sayyed, M.; Kothan, S.; Kaewkhao, J. Effect of BaO on Lead Free Zinc Barium Tellurite Glass for Radiation Shielding Materials in Nuclear Application. *J. Non-Cryst. Solids* **2020**, *550*, 120386. [CrossRef]
5. Sayyed, M.; Issa, S.A.; Büyükyıldız, M.; Dong, M. Determination of Nuclear Radiation Shielding Properties of Some Tellurite Glasses Using MCNP5 Code. *Radiat. Phys. Chem.* **2018**, *150*, 1–8. [CrossRef]
6. Sayyed, M.; Dong, M.; Tekin, H.; Lakshminarayana, G.; Mahdi, M. Comparative Investigations of Gamma and Neutron Radiation Shielding Parameters for Different Borate and Tellurite Glass Systems Using WinXCom Program and MCNPX Code. *Mater. Chem. Phys.* **2018**, *215*, 183–202. [CrossRef]
7. Al-Hadeethi, Y.; Sayyed, M.; Tijani, S. Gamma Radiation Attenuation Properties of Tellurite Glasses: A Comparative Study. *Nucl. Eng. Technol.* **2019**, *51*, 2005–2012. [CrossRef]
8. Kavaz, E.; Tekin, H.; Kilic, G.; Susoy, G. Newly Developed Zinc-Tellurite Glass System: An Experimental Investigation on Impact of Ta_2O_5 on Nuclear Radiation Shielding Ability. *J. Non-Cryst. Solids* **2020**, *544*, 120169. [CrossRef]
9. Tijani, S.; Kamal, S.M.; Al-Hadeethi, Y.; Arib, M.; Hussein, M.; Wageh, S.; Dim, L. Radiation Shielding Properties of Transparent Erbium Zinc Tellurite Glass System Determined at Medical Diagnostic Energies. *J. Alloy. Compd.* **2018**, *741*, 293–299. [CrossRef]
10. Rammah, Y.S. Evaluation of radiation shielding ability of boro-tellurite glasses: TeO_2–B_2O_3–$SrCl_2$–LiF–Bi_2O_3. *Appl. Phys. A* **2019**, *125*, 1–11. [CrossRef]
11. Almasbek, A.; Kozlovskiy, A.; Zdorovets, M. The Effect of Doping With Gallium and Indium Oxides on the Optical and Shielding Characteristics of $0.5TeO_2$-(0.5-2x)MoO_3-xGa_2O_3-xIn_2O_3 Glasses. *Opt. Mater.* **2021**, *118*, 111271. [CrossRef]
12. Al-Buriahi, M.S.; Mann, K.S. Radiation Shielding Investigations for Selected Tellurite-Based Glasses Belonging to the TNW System. *Mater. Res. Express* **2019**, *6*, 105206. [CrossRef]
13. Alalawi, A.; Al-Buriahi, M.; Sayyed, M.; Akyildirim, H.; Arslan, H.; Zaid, M.; Tonguc, B. Influence of Lead and Zinc Oxides on the Radiation Shielding Properties of Tellurite Glass Systems. *Ceram. Int.* **2020**, *46*, 17300–17306. [CrossRef]
14. Mhareb, M.H.A.; Alajerami, Y.S.M.; Dwaikat, N.; Al-Buriahi, M.S.; Alqahtani, M.; Alshahri, F.; Saleh, N.; Alonizan, N.; Saleh, M.A.; Sayyed, M.I. Investigation of photon, neutron and proton shielding features of H_3BO_3–ZnO–Na_2O–BaO glass system. *Nucl. Eng. Technol.* **2021**, *53*, 949–959. [CrossRef]
15. Gaballah, M.; Issa, S.A.M.; Saddeek, Y.B.; Elsaman, R.; Susoy, G.; Erguzel, T.T.; Alharbi, T.; Tekin, H.O. Mechanical and Nuclear Radiation Shielding Properties of Different Boro-Tellurite Glasses: A Comprehensive Investigation on Large Bi_2O_3 Concentration. *Phys. Scr.* **2020**, *95*, 085701. [CrossRef]
16. Issa, S.; Sayyed, M.; Kurudirek, M. Investigation of Gamma Radiation Shielding Properties of Some Zinc Tellurite Glasses. *J. Phys. Sci.* **2016**, *27*, 97–119. [CrossRef]
17. Hanfi, M.; Sayyed, M.; Lacomme, E.; Akkurt, I.; Mahmoud, K. The Influence of MgO on the Radiation Protection and Mechanical Properties of Tellurite Glasses. *Nucl. Eng. Technol.* **2021**, *53*, 2000–2010. [CrossRef]
18. Al-Buriahi, M.; Sayyed, M.; Al-Hadeethi, Y. Role of TeO2 in Radiation Shielding Characteristics of Calcium Boro-Tellurite Glasses. *Ceram. Int.* **2020**, *46*, 13622–13629. [CrossRef]
19. Sayyed, M.I.; Akyildirim, H.; Al-Buriahi, M.S.; Lacomme, E.; Ayad, R.; Bonvicini, G. Oxyfluoro-Tellurite-Zinc Glasses and the Nuclear-Shielding Ability under the Substitution of AlF_3 by ZnO. *Appl. Phys. A* **2020**, *126*, 88. [CrossRef]
20. Wood, J. *Computational Methods in Reactor Shielding*, 1st ed.; Elsevier BV: Amsterdam, The Netherlands, 1982.
21. Chilton, A.B.; Shultis, J.K.; Faw, R.E. *Principles of Radiation Shielding*; Prentice-Hall: Englewood Cliffs, NJ, USA, 1984.